DOI: 10.1002/anie.201108936

Photocatalytic CO_2 Conversion

Hybrid CuO-$TiO_{2-x}N_x$ Hollow Nanocubes for Photocatalytic Conversion of CO_2 into Methane under Solar Irradiation**

*Su-Il In, Dimitri D. Vaughn II, and Raymond E. Schaak**

Carbon dioxide is a greenhouse gas of growing concern, and its atmospheric concentration continues to rise from the ongoing burning of fossil fuels.[1] Catalysts that use sunlight to convert CO_2 into hydrocarbons and other fuels are attractive to help mitigate this problem, because they are able to simultaneously consume waste CO_2 and generate useful sources of energy in a sustainable and carbon-neutral manner.[1,2] TiO_2-based materials are the most common photocatalysts for CO_2 conversion, but they require either ultraviolet light because of the large band gap, anion doping to shift the band gap into the visible spectrum, or co-catalysts such as platinum that transfer electrons from the TiO_2 conduction band to the adsorbed CO_2.[2–8] An alternative strategy is to couple TiO_2 to CuO, which is a p-type semiconductor ($E_g = 1.35$–1.7 eV) with a valence band energy that lies near the CO_2/O_2 potential.[2,9] Such hybrid systems form p-n heterojunctions that have enhanced stability against photocorrosion, a higher separation of photogenerated charge carriers, and band edge alignments that are suitable for direct photocatalytic CO_2 conversion.[2,9–16] Furthermore, TiO_2 and CuO are both comprised of inexpensive elements that are abundant in the earth's crust.

Hybrid TiO_2 and Cu_xO systems have been used to catalyze hydrogen evolution[11,13,17–18] and organic dye degradation,[10] as well as CO_2 reduction to carboxylates[9] and hydrocarbons.[2,19] These systems are typically fabricated using chemical and physical deposition methods that effectively integrate TiO_2 and Cu_xO, but they do not generally permit simultaneous and rigorous control over nanostructure, dispersion, surface area, and heterojunction density. Such features are desirable for tuning and optimizing catalytic performance. Herein, we describe the design and synthesis of a new nanostructured material, hollow CuO nanocubes decorated with nanoparticles of titanium oxynitride ($TiO_{2-x}N_x$), that photocatalytically converts CO_2 into methane at ambient temperature and without platinum co-catalysts. The ability to incorporate nitrogen into TiO_2, which has not previously been accomplished in related hybrid nanostructures made using such low-temperature methods, is important because it helps to widen the wavelength range of solar radiation that can be absorbed.

Our design strategy, shown in Figure 1a, uses uniform colloidal Cu_3N nanocubes as reactive templates that define both the morphology and composition of the CuO-$TiO_{2-x}N_x$ product. First, Cu_3N nanocubes are synthesized by thermally decomposing $Cu(NO_3)_2$ in octadecylamine at 240 °C using

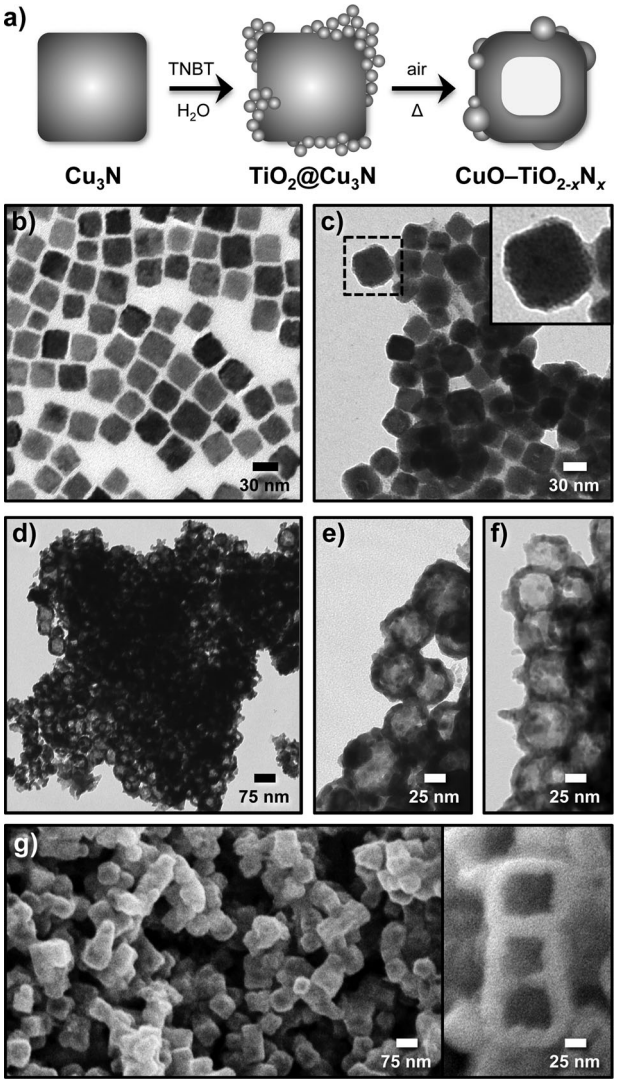

Figure 1. a) Diagram showing the multistep template strategy that converts Cu_3N nanocubes into hybrid TiO_2@Cu_3N nanocubes and CuO-$TiO_{2-x}N_x$ hollow nanocubes. TNBT = titanium *n*-butoxide. b–f) TEM images of: b) Cu_3N nanocubes; c) TiO_2@Cu_3N nanocubes; d–f) CuO-$TiO_{2-x}N_x$ hollow nanocubes; g) FESEM images of the CuO-$TiO_{2-x}N_x$ hollow nanocubes.

[*] Dr. S. I. In, D. D. Vaughn II, Prof. R. E. Schaak
Department of Chemistry and Materials Research Institute
The Pennsylvania State University
University Park, PA 16802 (USA)
E-mail: schaak@chem.psu.edu

[**] This work was supported by a Scialog Award to R.E.S. from the Research Corporation for Science Advancement. TEM imaging was performed in the Electron Microscopy Facility of the Huck Institutes of the Life Sciences and at the Materials Characterization Lab at the Penn State Materials Research Institute. The authors also thank Vince Bojan for acquisition of the XPS data.

Supporting information for this article is available on the WWW under http://dx.doi.org/10.1002/anie.201108936.

a minor modification of two recent reports[20,21] (see the Experimental Section for details). The transmission electron microscope (TEM) image in Figure 1b shows the resulting uniform (27.3 ± 3.3) nm cubes. Selected area electron diffraction (SAED) and powder X-ray diffraction (XRD) data (Supporting Information, Figure S1) confirm that the nanocubes are Cu_3N. Next, amorphous TiO_2 is deposited on the Cu_3N nanocube surfaces by the slow hydrolysis of titanium *n*-butoxide (TNBT). A TEM image of the resulting TiO_2@Cu_3N nanocubes is shown in Figure 1c.

The TiO_2@Cu_3N nanocubes are then collected as a powder and annealed at 450 °C for 1 h in air. Several aspects of this annealing process are important for converting the TiO_2@Cu_3N nanocubes into the final CuO-$TiO_{2-x}N_x$ hollow nanocube products. First, the TiO_2 crystallizes and fuses to the nanocube surface. As TiO_2 does not fully passivate the Cu_3N surface, the Cu_3N is accessible to oxygen. Cu_3N therefore reacts with oxygen to form hollow CuO nanocubes through a putative Kirkendall mechanism,[22] where the inward diffusion of oxygen is presumably slower than the outward diffusion of nitrogen. At the same time, the TiO_2 crystallizes and fuses to the nanocube surface. While it does not fully encapsulate the nanocube, it helps to retain the nanocube morphology throughout the annealing process. Indeed, control experiments show that thermal oxidation of Cu_3N nanocubes without attached TiO_2 results in irregularly shaped and agglomerated CuO nanostructures, with no morphological retention (Supporting Information, Figure S2). Finally, the nitrogen species that diffuses outward from the Cu_3N template is able to react with the crystallizing TiO_2 on the nanocube surface, forming $TiO_{2-x}N_x$ at 450 °C.

TEM images of the final product (Figure 1d–f) show that it consists of hollow (56.8 ± 7.6) nm CuO nanocubes with truncated corners, porous outer shells, and small particles of $TiO_{2-x}N_x$ decorating the surface. The field emission scanning electron microscope (FESEM) image in Figure 1g confirms the nanocube morphology, the size uniformity, and the hollow interior. The high-resolution TEM (HRTEM) image in Figure 2a shows the edge of a representative CuO-$TiO_{2-x}N_x$ nanoparticle. Two distinct lattice spacings are observed in the particles that comprise the nanocube surface: 2.7 Å, which uniquely corresponds to CuO (110), and 3.5 Å, which uniquely corresponds to anatase $TiO_{2-x}N_x$ (101); the lattice constants of TiO_2 and $TiO_{2-x}N_x$ are effectively indistinguishable. The sizes of the $TiO_{2-x}N_x$ particles are in the range of 5–10 nm. The SAED pattern in Figure 2b shows spots that also correspond to CuO (110) and $TiO_{2-x}N_x$ (101). Figure 2c shows a dark-field scanning transmission electron microscope (STEM) image of several CuO-$TiO_{2-x}N_x$ hollow nanocubes. Element distribution maps for Cu (Figure 2d) and Ti (Figure 2e), generated from electron energy-loss spectroscopy (EELS) data, indicate that Cu is distributed uniformly around the hollow nanocubes, whereas Ti is present in smaller clusters that surround the Cu regions. A thin film of the CuO-$TiO_{2-x}N_x$ hollow nanocubes also shows a clear photo-switching response under light and dark conditions (Supporting Information, Figure S3), which is characteristic of a p-n junction and provides electrochemical evidence for the presence of CuO-$TiO_{2-x}N_x$ heterojunction interfaces throughout the material. The EELS data for this nanocube indicate a Cu/Ti atomic ratio of 98:2, and energy dispersive spectroscopy (EDS) data from a larger area confirm the distribution of Cu and Ti throughout the sample (Figure S4). Similarly, inductively coupled plasma atomic emission spectrometry (ICP-AES) data indicate a Ti concentration that corresponds to 4.7 wt % TiO_2 throughout the sample. Powder XRD data (Supporting Information, Figure S5) show evidence of CuO but not $TiO_{2-x}N_x$; this is consistent with the small amount of $TiO_{2-x}N_x$ that is present relative to CuO, which is below the XRD detection limit. Taken together, these data are consistent with polycrystalline, porous nanocubes of CuO that are decorated with small nanoparticles of $TiO_{2-x}N_x$.

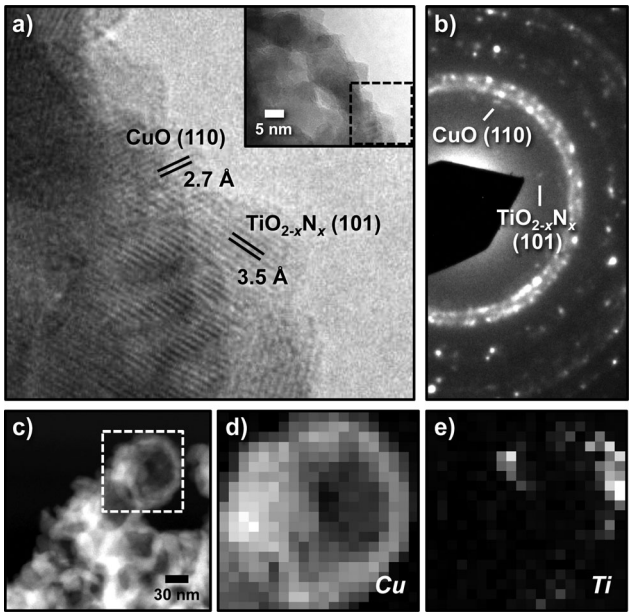

Figure 2. a) HRTEM image showing the presence of adjoined CuO and $TiO_{2-x}N_x$ on the nanocube surface. A zoomed-out TEM image is shown in the inset, with the dashed box indicating the region shown in the main panel. b) SAED pattern corresponding to the sample shown in panel (a). c) Dark-field STEM image of the CuO-$TiO_{2-x}N_x$ hollow nanocubes with element mapping images for Cu (d) and Ti (e) that correspond to the region highlighted by the dashed box in panel (c).

UV/Vis diffuse reflectance spectra for CuO and CuO-$TiO_{2-x}N_x$ appear similar, with an onset of absorption near 600 nm that corresponds to CuO (Figure 3a). The band gap energy estimated by Kubelka–Munk transformation of the diffuse reflectance data (Supporting Information, Figure S6) is 1.44 eV, which is within the range of reported band gap energies for CuO (1.35–1.7 eV).[23] The CuO-$TiO_{2-x}N_x$ hollow nanocubes absorb more in the 350–500 nm range than the CuO standard, which suggests that the $TiO_{2-x}N_x$ component contributes to the absorbance below 500 nm. Anatase TiO_2, which has a band gap of 3.2 eV, typically absorbs only below 400 nm, but nitrogen incorporation into TiO_2 is known to extend the absorption edge to longer wavelengths.[24–26] Therefore, the increased absorbance below 500 nm is consistent with the presence of some nitrogen-substituted TiO_2.

Further evidence for the presence of $TiO_{2-x}N_x$ comes from X-ray photoelectron spectroscopy (XPS) data. Figures 3b and c show XPS spectra for the O 1s and N 1s regions, respectively.

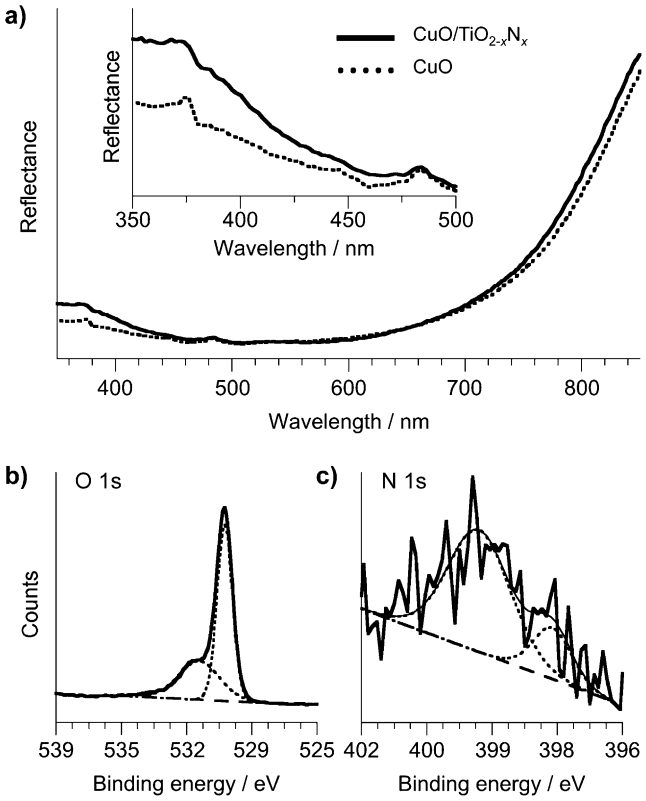

Figure 3. a) UV/Vis diffuse reflectance spectra for the CuO-$TiO_{2-x}N_x$ nanocubes and the CuO control sample. b, c) XPS spectra of the CuO-$TiO_{2-x}N_x$ hollow nanocubes showing the O 1s (b) and N 1s (c) regions, showing the experimental data (——), the peak deconvolution (•••••), and the fitted background (–•–•).

The O 1s region shows peaks near 529.9 eV and 531.3 eV. Prior XPS studies of $TiO_{2-x}N_x$ have attributed the peak near 530 eV to Ti–O (for example, TiO_2) and the peak near 531.5 eV to Ti–*N*–O (for example, $TiO_{2-x}N_x$). A small above-baseline contribution near 534 eV is attributed to chemisorbed oxygen, perhaps from residual oxidized hydrocarbons.[27,28] The N 1s region is much noisier, but the shape of the above-baseline signal is more consistent with a contribution from two peaks rather than one. The first peak, centered between 398.5 and 400 eV, is typically associated with chemisorbed nitrogen,[28] and is likely attributable to residue that remains from the alkylamine stabilizer. Contributions in the range of 396–398.5 eV, which is where the second above-baseline feature is located, have previously been attributed to Ti–N and Ti–N–O, and is consistent with $TiO_{2-x}N_x$.[24,25,28,29] XPS data for the Cu 2p and Ti 2p regions are shown in the Supporting Information (Supporting Information, Figure S7), and they confirm the presence of Cu^{2+} and Ti^{4+}. The amount of nitrogen incorporated into the TiO_2 is small, as is the phase fraction of $TiO_{2-x}N_x$ relative to CuO, and therefore quantitation of the nitrogen content is not possible. However, the UV/Vis and XPS data are both consistent with the formation of a hybrid nanostructure containing CuO and TiO_2 that includes some substituted nitrogen.

Photocatalytic CO_2 conversion measurements were carried out under simulated solar irradiation (AM 1.5 G, 100 mW c^{2-2}) at ambient temperature, and reaction products

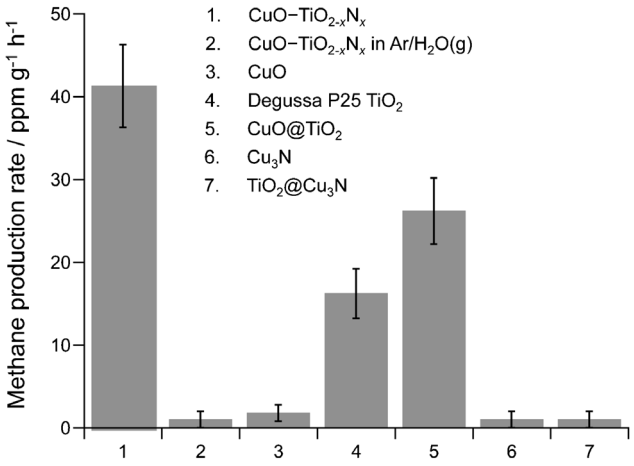

Figure 4. Rates of methane production (ppm $g^{-1}h^{-1}$) under solar irradiation for the CuO-$TiO_{2-x}N_x$ hollow nanocubes in CO_2/H_2O(g) and Ar/H_2O(g), along with data from CuO, TiO_2, CuO@TiO_2, Cu_3N, and TiO_2@Cu_3N control samples in CO_2/H_2O(g).

were monitored by gas chromatography (GC). Degussa P25 TiO_2, a commercial benchmark material, and CuO made by annealing the Cu_3N nanocubes without TiO_2 (Supporting Information, Figure S2) were used as reference samples. GC analysis of the products showed predominantly methane, along with ethane, propane, and butane as minor products. Figure 4 shows the methane formation rates for each sample, plus additional controls. The CuO-$TiO_{2-x}N_x$ hollow nanocubes yield 41.3 ppm $g^{-1}h^{-1}$ of methane, which represents a production rate that is 2.5 times faster than that of Degussa P25 TiO_2 when measured under the same conditions (16.2 ppm $g^{-1}h^{-1}$). The CuO sample showed negligible activity. An additional control sample, made by a traditional impregnation route to CuO@TiO_2,[11,17] yielded a methane production rate of 26.2 ppm $g^{-1}h^{-1}$. This result is an improvement relative to Degussa P25 TiO_2 without CuO, but does not approach the rate obtained using the cube-shaped nitrogen-containing CuO-$TiO_{2-x}N_x$ particles. When normalized to the measured Brunauer–Emmett–Teller (BET) surface areas of the samples (24 m^2g^{-1} for CuO-$TiO_{2-x}N_x$, 50 m^2g^{-1} for Degussa P25 TiO_2, and 31 m^2g^{-1} for CuO@TiO_2 made by impregnation), the methane production rate of the hollow CuO-$TiO_{2-x}N_x$ nanocubes is four times faster than that of the TiO_2 standard and two times faster than that of the CuO@TiO_2 control. There is no improvement in the photocatalytic activity when the amount of $TiO_{2-x}N_x$ in the CuO-$TiO_{2-x}N_x$ nanocubes is increased by a factor of three. We hypothesize that excessive TiO_2 may minimize access to the surface active sites around the p-n junctions, as it is known that efficiency and selectivity in the photocatalytic reduction of CO_2 depend strongly on the type of active sites.[30] Also, control experiments show that there is no appreciable hydrocarbon production in the absence of either solar irradiation or photocatalysts, indicating that there are no significant thermal or photon effects, respectively. When tested in Ar/H_2O(g) instead of CO_2/H_2O(g), CuO-$TiO_{2-x}N_x$ shows no evidence of hydrocarbon production beyond the background noise of the measurement, suggesting that any organic impurities on the surface of the CuO-$TiO_{2-x}N_x$ particles have negligible

involvement in the CO_2 conversion reaction or on the reported methane production rates. Cu_3N and TiO_2@Cu_3N also show negligible methane production.

It is difficult to directly compare the methane production rate of the CuO-$TiO_{2-x}N_x$ hollow nanocubes with rates reported for other photocatalysts because of the variance in experimental conditions, morphological features, surface areas, and co-catalysts. However, the catalytic performance of the CuO-$TiO_{2-x}N_x$ hollow nanocubes is comparable to, and perhaps better than, other reported photocatalysts that convert CO_2 into methane using solar irradiation and without using noble metal co-catalysts, including $NaNbO_3$ (22 ppm g^{-1} h^{-1}),[31] TiO_2 nanotube arrays (10 ppm),[8] and Zn_2GeO_4 nanorods (3.5 ppm h^{-1}).[32]

In conclusion, we have described a multi-template strategy for synthesizing hollow nanocubes of CuO-$TiO_{2-x}N_x$, a new hybrid material that photocatalytically converts CO_2 into methane under solar irradiation. The synthetic strategy uses uniform Cu_3N nanocubes as both a morphological and compositional template for subsequent deposition of a partial TiO_2 shell, oxidation of the Cu_3N core to form hollow CuO nanocubes, and low-temperature (450 °C) incorporation of the expelled nitrogen into the TiO_2 framework to form crystalline $TiO_{2-x}N_x$. Given this synthetic strategy and the design parameters that can be systematically varied, it should be possible to further improve the catalytic performance and to better understand nanostructure–property correlations in these and related materials.

Experimental Section

Synthesis of CuO-$TiO_{2-x}N_x$: Cu_3N nanocubes were synthesized by heating $Cu(NO_3)_2$·$3H_2O$ (0.3 g) and ODA (10 mL) to 240 °C for 10 min with magnetic stirring, then cooling to 80 °C, adding warm ethanol (20 mL; 60 °C), and continuing to stir for 1 h. The Cu_3N nanocubes were collected by centrifugation (ca. 3000 rpm, 5 min), washed several times with warm ethanol, dispersed in cyclohexane, and dried under vacuum. The isolated Cu_3N nanocubes (10 mg) were then dispersed in ethanol (15 mL) and mixed with poly(n-vinyl pyrrolidone) K-30 (PVP, 0.1 g) with magnetic stirring. After 10 min, titanium n-butoxide (TNBT, 0.02 mL) was added, followed by dropwise addition of water (0.1 mL) in ethanol (5 mL). The product was collected by centrifugation, dried at 70–80 °C for 1 h, and heated at 450 °C for 1 h (ramp rate, 2 °C min^{-1}). Instrumental characterization details are included in the Supporting Information.

Catalytic testing: Details of the reactor setup are included in the Supporting Information. After loading the sample (100 mg), the reaction chamber was evacuated to about 40 mTorr. Pure CO_2 (99.95 %) was introduced into the chamber through a deionized water bubbler at a total flow rate of 3.18 mL min^{-1}. The CO_2 loading/evacuation process was repeated five times. The relative standard deviation of the CO_2 concentration was about 1.5 %, and the relative humidity was measured to be about 80 %. A 300 W Xe lamp with an AM1.5 filter was used as a light source (light intensity: 100 mW cm^{-2}). After the photocatalytic reaction was allowed to proceed for three hours, quantitative detection of reactants and products was performed using a Shimadzu GC-2014 gas chromatograph (Restek Rt-Q-Bond column, ID = 0.53 mm, length = 30 m) equipped with flame ionization (FID) and thermal conductivity (TCD) detectors.

Received: December 19, 2011
Revised: January 17, 2012
Published online: March 5, 2012

Keywords: copper oxide · sustainable fuels · nanostructures · photocatalysts · titanium dioxide

[1] Z. Jiang, T. Xiao, V. L. Kuznetsov, P. P. Edwards, *Philos. Trans. R. Soc. London Ser. A* **2010**, *368*, 3343 – 3364.
[2] S. C. Roy, O. K. Varghese, M. Paulose, C. A. Grimes, *ACS Nano* **2010**, *4*, 1259 – 1278.
[3] X. Feng, J. D. Sloppy, T. J. LaTempa, M. Paulose, S. Komarneni, N. Bao, C. A. Grimes, *J. Mater. Chem.* **2011**, *21*, 13429 – 13433.
[4] C. Wang, R. L. Thompson, J. Baltrus, C. Matranga, *J. Phys. Chem. Lett.* **2010**, *1*, 48 – 53.
[5] M. Anpo, H. Yamashita, Y. Ichihashi, Y. Fujii, M. Honda, *J. Phys. Chem. B* **1997**, *101*, 2632 – 2636.
[6] O. Ozcan, F. Yukruk, E. U. Akkaya, D. Uner, *Top. Catal.* **2007**, *44*, 523 – 528.
[7] Q.-H. Zhang, W.-D. Han, Y.-J. Hong, J.-G. Yu, *Catal. Today* **2009**, *148*, 335 – 340.
[8] O. K. Varghese, M. Paulose, T. J. LaTempa, C. A. Grimes, *Nano Lett.* **2009**, *9*, 731 – 737.
[9] S. Qin, F. Xin, Y. Liu, X. Yin, W. Ma, *J. Colloid Interface Sci.* **2011**, *356*, 257 – 261.
[10] N. Helaïli, Y. Bessekhouad, A. Bouguelia, M. Trari, *J. Hazard. Mater.* **2009**, *168*, 484 – 492.
[11] J. Bandara, C. P. K. Udawatta, C. S. K. Rajapakse, *Photochem. Photobiol. Sci.* **2005**, *4*, 857 – 861.
[12] D. Barreca, G. Carraro, V. Gombac, A. Gasparotto, C. Maccato, P. Fornasiero, E. Tondello, *Adv. Funct. Mater.* **2011**, *21*, 2611 – 2623.
[13] S. Xu, A. J. Du, J. Liu, J. Ng, D. D. Sun, *Int. J. Hydrogen Energy* **2011**, *36*, 6560 – 6568.
[14] S. Anandan, M. Miyauchi, *Phys. Chem. Chem. Phys.* **2011**, *13*, 14937 – 14945.
[15] X. Qiu, M. Miyauchi, H. Yu, H. Irie, K. Hashimoto, *J. Am. Chem. Soc.* **2010**, *132*, 15259 – 15267.
[16] M. Liu, X. Qiu, M. Miyauchi, K. Hashimoto, *Chem. Mater.* **2011**, *23*, 5282 – 5286.
[17] S. Xu, D. D. Sun, *Int. J. Hydrogen Energy* **2009**, *34*, 6096 – 6104.
[18] V. Gombac, L. Sordelli, T. Montini, J. J. Delgado, A. Adamski, G. Adami, M. Cargnello, S. Bernal, P. Fornasiero, *J. Phys. Chem. A* **2010**, *114*, 3916 – 3925.
[19] J. Yu, Y. Hai, M. Jaroniec, *J. Colloid Interface Sci.* **2011**, *357*, 223 – 228.
[20] D. Wang, Y. Li, *Chem. Commun.* **2011**, *47*, 3604 – 3606.
[21] H. Wu, W. Chen, *J. Am. Chem. Soc.* **2011**, *133*, 15236 – 15239.
[22] Y. D. Yin, R. M. Rioux, C. K. Erdonmez, S. Hughes, G. A. Somorjai, A. P. Alivisatos, *Science* **2004**, *304*, 711 – 714.
[23] F. P. Koffyberg, F. A. Benko, *J. Appl. Phys.* **1982**, *53*, 1173 – 1177.
[24] S.-I. In, P. C. K. Vesborg, B. L. Abrams, Y. Hou, I. Chorkendorff, *J. Photochem. Photobiol. A* **2011**, *222*, 258 – 262.
[25] S.-I. In, A. Orlov, F. Garcia, M. Tikhov, D. S. Wright, R. M. Lambert, *Chem. Commun.* **2006**, 4236 – 4238.
[26] K. Maeda, K. Domen, *J. Phys. Chem. C* **2007**, *111*, 7851 – 7861.
[27] A. Trenczek-Zajac, M. Radecka, K. Zakrzewska, A. Brudnik, E. Kusior, S. Bourgeois, M. C. Marco de Lucas, L. Imhoff, *J. Power Sources* **2009**, *194*, 93 – 103.
[28] M.-H. Chan, F.-H. Lu, *Thin Solid Films* **2009**, *517*, 5006 – 5009.
[29] O. Diwald, T. L. Thompson, T. Zubkov, E. G. Goralski, S. D. Walck, J. T. Yates, Jr., *J. Phys. Chem. B* **2004**, *108*, 6004 – 6008.
[30] H. Yamashita, N. Kamada, H. He, K. Tanaka, S. Ehara, M. Anpo, *Chem. Lett.* **1994**, 855 – 858.
[31] H. Shi, T. Wang, J. Chen, C. Zhu, J. Ye, Z. Zou, *Catal. Lett.* **2011**, *141*, 525 – 530.
[32] S. Yan, L. Wan, Z. Li, Z. Zou, *Chem. Commun.* **2011**, *47*, 5632 – 5634.

